# Modular Energy Cost Optimization for Buildings with Integrated Microgrid

Vinko Lešić[a,*], Anita Martinčević[b], Mario Vašak[c]
[a,b,c]Laboratory for Renewable Energy Systems
University of Zagreb, Faculty of Electrical Engineering and Computing
Unska 3, HR-10000 Zagreb, Croatia
[a]vinko.lesic@fer.hr ([*]corresponding author), [b]anita.martincevic@fer.hr, [c]mario.vasak@fer.hr

***Abstract*—Buildings are becoming suitable for application of sophisticated energy management approaches to increase their energy efficiency and possibly turn them into active energy market participants. The paper proposes a modular coordination mechanism between building zones comfort control and building microgrid energy flows control based on model predictive control. The approach opens possibilities to modularly coordinate technologically heterogeneous building subsystems for economically-optimal operation under user comfort constraints. The imposed modularity is based on a simple interface for exchanging building consumption and microgrid energy price profiles. This is a key element for technology separation, replication and up-scaling towards the levels of smart grids and smart cities where buildings play active roles in energy management. The proposed coordination mechanism is presented in a comprehensive realistic case study of maintaining comfort in an office building with integrated microgrid. The approach stands out with significant performance improvements compared to various non-coordinated predictive control schemes and baseline controllers. Results give detailed information about yearly cost-effectiveness of the considered configurations, which are suitable for deployment as short- and long- term zero-energy building investments.**

***Index Terms*—Buildings energy management, Zone comfort control, Energy-efficiency, Microgrid energy management, Volatile pricing, Hierarchical model predictive control.**

## I. Introduction

With 40% of total primary energy spent for buildings operation, numerous policies and initiatives directed towards their energy efficiency increase have emerged. The EU *2030 Energy Strategy*, built on promising results and well-adopted research and implementation trends of the previous 20-20-20 strategy ($CO_2$ reduction - renewables share - energy savings), targets towards 40-27-27 by the end of year 2030 [1]. A significant focus is put on the buildings sector as the largest energy consumer. Ongoing research on smart grids, systems of systems and internet of things created an opportunity to push savings further with systematic improvements of electrical, heating or water supply systems. This economical motivation brought highly efficient building categories such as *Energy Star* (USA) or *Passivhaus Standard* (EU), with the final goal of reaching *Zero-energy buildings* and implied inclusion of distributed power generation and storage units [1]. Integration of these thoroughly diverse complex systems is enabled by high-level management methods where model predictive control (MPC) has emerged as a promising optimal and flexible technique [2].

Application of the MPC to building energy management had a great impact on research trends and contributed with experimentally validated building energy efficiency increase by 17% [3] to 28% [4] (theoretically expected up to 70% [5] in particular comprehensive applications), heat pump energy savings of 13% [6], load shifting possibility [7] for power grid balancing or additional economic savings with hourly-variable electricity prices [8]. Furthermore, introduction of microgrid with distributed power generation and storage units allows buildings to enter the energy market as active participants and ensure revenues [9] with bidding strategies, where increase in profit is achieved with combined microgrid and building climate control (e.g. by about 15% in [10]). With inherent ability to handle constraints, MPC has lead to the system reliability and improvement of users comfort at the same time when compared with state-of-the-art adopted control methods. This is also expected to contribute to productivity within commercial buildings. A motivation for integration of all building subsystems towards the energy efficiency and cost-effectiveness increase is evident.

Simultaneous building thermal comfort satisfaction and smart grid demand response management is addressed in [7], [11], [12]. The papers illustrate an opportunity of utilizing buildings to resolve the critical issue of power imbalance in the distribution grid. Buildings act as thermo-electric storage systems, which are identified as the main need for integration of large share of renewable energy sources [13].

Buildings are complex systems composed of many subunits responsible for maintaining safe and steady operation such as: sensors, thermal actuators, zone (room/office) climate controllers, central heating/cooling medium production units, medium supply ducts, lighting, shading, fire alarms and security systems. Recently, photovoltaic systems, wind turbines, energy storage units with corresponding charging curves are also included in the form of a microgrid. These subsystems are all very different in dynamics, priorities, means of operation but also implementation aspects such as energy levels, protocols, maintenance services etc. Rather than having one large control structure to handle all the subsystems at once, it is more natural to separate it into subunits in a hierarchical or distributed way [14], [15], [16]. In addition, many of the listed subsystems can be subjected to optimization methods, and many of them already have such algorithms implemented.

Examples of recent contributors in general control theory and distributed control topics are in topological approach of robust hierarchical control [14] or solvers efficiency increase with decentralized active-set method [17] for systems with

**Nomenclature**

*Acronyms*

| | |
|---|---|
| COP | coefficient of performance |
| CR | critical region |
| EER | energy efficiency ratio |
| HVAC | heating, ventilation and air conditioning |
| LP | linear program |
| MPC | model predictive control |
| RC | resistance-capacitance |
| SoC | state-of-charge |
| SP | temperature setpoint |

*Symbols*

| | |
|---|---|
| $A$ | state matrix |
| $B$ | input matrix |
| $C$ | storage capacity |
| $c$ | price vector |
| $C^z$ | zone output matrix |
| $\gamma$ | trajectory following weight |
| $\Delta$ | allowed setpoint deviation |
| $\Delta$u | price sensitivity |
| $D$ | linear control law slope |
| $d$ | disturbance vector |
| $E$ | energy between two time instants |
| $\varepsilon$ | small value |
| $\eta$ | storage efficiency |
| $f$ | parameter weighting vector |
| $G$ | control constraints matrix |
| $g_1, g_2$ | penalty weighting factors |
| $h$ | control variable weighting vector |
| $J$ | cost function value |
| $L$ | parameter constraints matrix |
| $N$ | prediction horizon |
| $P$ | power |
| $Q$ | temperature weighting matrix |
| $q$ | linear control law offset |
| $r$ | zone control weighting factor |
| $\sigma_1, \sigma_2$ | penalty slack variables |
| $T$ | temperature |
| $T_s$ | sampling time |
| $\theta$ | optimization parameter |
| $u$ | control vector |
| $w$ | constraints vector |
| $x$ | state vector |
| $y$ | output vector |

*Superscripts*

| | |
|---|---|
| $*$ | energy-optimal value |
| $**$ | price-optimal value |
| A | active constraints |
| BAT | battery variable |
| FC | hydrogen storage variable |
| G | grid variable |
| NA | inactive constraints |
| L | microgrid load |
| $\mu$ | microgrid level variable |
| PV | photovoltaic array variable |
| WT | wind turbine variable |
| $z$ | zone level variable |

*Subscripts*

| | |
|---|---|
| 0 | initial condition |
| ch | charging |
| CR | critical region |
| dch | discharging |
| $k$ | time instant |
| o | outside conditions |
| T | temperature-related variable |

communication delays or in distributed alternating direction method of multipliers [18].

A significant feature in building applications is observed in a proximity of energy and economical optimum ([7], [8]). The method proposed in this work exploits the proximity premise for dividing a problem into hierarchy levels suitable for fast convergence from low level optimization criterion to the higher one. With parametric formulation, both criteria are expected in the same or adjacent critical region (CR) while shifting between them is trivial in complexity and time requirements. Hence, the system independency and algorithm time efficiency are gained at the same time. Lower hierarchy level control variables are treated as a parametric disturbance of the higher hierarchy level problem and further transformed towards global optimization criterion through a parametric problem value function. The proposed hierarchical decomposition introduces also computational relaxation and algorithm efficiency, but the main contribution is to keep the microgrid and zone level technologies apart and independent (see Fig. 1). The implementation is therefore eased with minimal on-site modifications and different technologies are interconnected only by means of provided price and consumption signals. This reflects to significant cost reduction since the equipment integration and required expert staff knowledge is identified as the most pronounced contributor of implementation expenses [3].

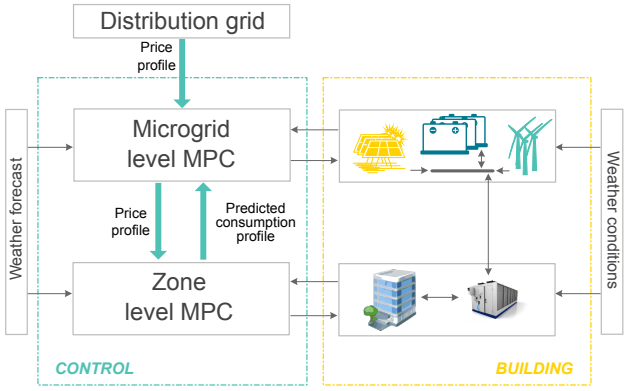


Fig. 1. Modular zone and microgrid control illustration.

The paper is focused on integration of several energy systems for major mutual cost saving opportunities, applied to building climate control with integrated microgrid. The following contributions are highlighted: $(i)$ proposition of modular hierarchical MPC method for system coordination through predicted energy consumption and corresponding prices, and $(ii)$ detailed realistic simulations performed on the chosen test site of building with integrated microgrid in real (non-averaged) weather and market conditions and numerous scenarios. Results give a reliable estimate of building climate and microgrid operation costs with applied simple and more sophisticated controllers including the proposed coordinated modular MPC.

The proposed method is applied to a particular case of a building with integrated microgrid, where building zone heating/cooling is coordinated with renewable energy production, storages state of charge and volatile electricity pricing from the electricity distribution grid. The microgrid level MPC maintains cost-optimal energy balance of the microgrid and the zone level MPC maintains the zone temperature comfort in energy-

optimal way. In the proposed coordinated operation, microgrid level MPC receives predicted energy consumption profiles from the zone level MPC and issues back the optimized price profile relevant for the predicted consumption (see Fig. 1). The optimized price profile includes information on how a zone level energy consumption change reflects on the overall building energy cost while taking into account the optimized microgrid operation. The approach stands out with its modularity and easy switching between uncoordinated individual modules operation and coordinated control for mutual economic gain.

The modularity is also suitable for coordination extension to new vertical modules, e.g. central HVAC unit level between the current levels or aggregator and district levels on the grid side above the microgrid level. Following the same established methodology, levels are coordinated by information on a predicted consumption in the up direction and issuing a price for the received predicted consumption in the down direction. In case of absent modules, the remaining ones are still coordinated via the matching interfaces for achieving the economical optimum in the current system configuration. The approach is readily applicable for buildings and grids operating in various conditions: different climates, building zone topologies, thermal actuator types or additional microgrid components, including controllable or non-controllable loads.

The paper gives a comparison of several control and energy management approaches applied to a case study of 23 offices at University of Zagreb Faculty of Electrical Engineering and Computing (UniZG-FEEC) with two-pipe fan coil units and integrated 48 V DC microgrid, which consists of photovoltaic array, wind turbine, battery and hydrogen-based storage system with fuel cells. In the presented scenarios, building cooling/heating process is the only load of the microgrid. Thorough simulations are performed using the site weather data for 2014 provided by Croatian Meteorological and Hydrological Service, volatile energy market electricity prices taken from European Power Exchange company portal [19], building construction material parameters for thermal zone models, and parameters of commercial microgrid components. Performed simulations show how different configurations of MPC contribute to energy and cost savings under the current two-tariff and expected volatile electricity pricing scenarios. They are also a realistic prediction of how profitable in general each of the approaches would be for different building sites and scales in temperate climate areas.

The paper is organized as follows. Optimal control problem for high-comfort zone temperature regulation with the corresponding model of building thermal dynamics is presented in Section II. Microgrid energy flow optimization and storage dynamics are given in Section III. Section IV presents the proposed method of hierarchical MPC performed by parametric optimization. The case study is described in Section V. Section VI elaborates the application of MPC in different configurations to energy management for the case study. Simulation scenarios and results are presented and discussed in Section VII. Section VIII summarizes paper contributions.

## II. Building zones optimal control for high comfort demands

### A. Discrete-time system model

The most usual approach in thermal modeling of zones is based on a well established linear resistance-capacitance (RC) representation where each type of building surface (outside wall, window, inside wall, floor, roof etc.) is represented with few states (depending on the material properties and desired model accuracy). Examples of RC model applications in MPC can be found in [2], [5], [20].

The sampling time for the model discretization is usually paired with the sampling time of available weather forecast. For improving the model accuracy, influence of outdoor temperature ($T_o$) variation within the sampling time interval is included by linear interpolation of temperature between the current and the next sampling time instant ($k$ and $k+1$), as follows:

$$x^z_{k+1} = A^z x^z_k + B^z_u u^z_k + B^z_T T_{o,k} + B^{z+}_T T_{o,k+1} + B^z_d d^z_k, \quad \text{(1a)}$$

$$y^z_k = C^z x^z_k, \quad \text{(1b)}$$

where $k \in \mathbb{Z}$ is the sampling time index, $x^z_k \in \mathbb{R}^{n^z_x}$ is the system state vector, $u^z_k \in \mathbb{R}^{n^z_u}$ is the system input vector, i.e., vector of hourly thermal energy inputs from the thermal actuators to each of the $n^z_u$ controllable zones, $T_{o,k}$ is the outdoor air temperature, $d^z_k \in \mathbb{R}^{n^z_d}$ is the vector of $n^z_d$ disturbances that act on the system (e.g. hourly solar radiation on walls and windows, internal gains etc.) and $y^z_k \in \mathbb{R}^{n^z_y}$ is the system measurements vector, i.e., the vector of zone temperatures. System matrices $A^z$, $B^z_u$, $B^z_T$, $B^{z+}_T$, $B^z_d$ and $C^z$ describe building zones thermal dynamics and input-output relationships.

### B. Optimization problem

In this particular application, the goal of the MPC-operated climate control is to achieve the best possible user comfort with minimum energy consumption. Common approaches minimize the energy consumption within large temperature comfort span, supported by the recommendation of guidelines and rules [2], [21]. Productivity of occupants in commercial buildings depends largely on comfort levels, but also on lots of the subjective factors [22], [23], [24]. We therefore opt for tracking the user temperature setpoint with $\Delta = 0.5^\circ$C allowed deviation. This approach allows the individual setting of comfort level with the aim of user satisfaction and increased productivity rather than achieving additional energy savings. The distinct advantage of the proposed approach is a direct control of thermal energy inputs per zone. For this, the methodology is readily applicable for different thermal zone actuators and retains openness for interaction with other building subsystems.

The allowed deviation from the setpoint is put in the form of MPC soft constraints:

$$\begin{gathered} \mathrm{SP} - \Delta - \sigma_1 \le y^z \le \mathrm{SP} + \Delta + \sigma_2, \\ \sigma_1 \ge 0, \quad \sigma_2 \ge 0, \end{gathered} \quad (2)$$

where SP denotes temperature setpoint and coefficients $\sigma_1$ and $\sigma_2$ are slack variables that allow highly penalized constraints violation and feasible implementation.

The zone thermal actuator limitations are formulated as input constraints:

$$u^z_{\min} \leq u^z \leq u^z_{\max}, \tag{3}$$

where negative and positive signs of $u^z$ denote cooling and heating, and $u^z_{\min}$ and $u^z_{\max}$ are the maximum cooling and the maximum heating thermal energies attainable by thermal actuators within the sampling period, respectively. Total delivered thermal energy for the considered group of zones is also limited by the maximum possible supply ($u^{z,\text{tot}}_{\min}$ for cooling and $u^{z,\text{tot}}_{\max}$ for heating), which means the system is not necessarily designed to withstand the peak operation on all of its thermal actuators in zones:

$$u^{z,\text{tot}}_{\min} \leq \sum_{j=1}^{n_u} u^z_j \leq u^{z,\text{tot}}_{\max}, \tag{4}$$

where $j$ is the zone index.

Finally, the optimization problem is formulated as a reference tracking problem:

$$\begin{aligned} J^{z*} = \min_{\mathbf{u}^z, \boldsymbol{\sigma_1}, \boldsymbol{\sigma_2}} & \sum_{k=0}^{N-1} |r_k u^z_k| + \gamma \sum_{k=1}^{N} |r_k \mathrm{Q}_k (y^z_k - \mathrm{SP}_k)| + \\ & + \sum_{k=1}^{N} \left| g_{1_k}^\top \sigma_{1_k} \right| + \sum_{k=1}^{N} \left| g_{2_k}^\top \sigma_{2_k} \right|, \\ \text{s.t.} \quad & (1), (2), (3), (4) \end{aligned} \tag{5}$$

where $r_k \in \mathbb{R}^1$ is the energy cost important for subsequent coordination with the microgrid control, $g_{1_k} \in \mathbb{R}^{n^z_y}$ and $g_{2_k} \in \mathbb{R}^{n^z_y}$ are weighting parameters for tuning the optimization criterion. Matrix $\mathrm{Q}_k$ transforms temperature deviation from the setpoint to the corresponding thermal energy such that it is comparable to $u^z_k$ [25]. Bold notation for optimizers $\mathbf{u}^z, \boldsymbol{\sigma_1}, \boldsymbol{\sigma_2}$ stands for vectors stacked over the prediction horizon $N$. The parameter $\gamma$ is introduced for trade-off possibility of comfort-savings criterion. With $\gamma < 1$, the controller maintains the temperature at the $\pm\Delta$ boundary most of the time and large energy savings are directly a result of the deviation from setpoints. For $\gamma \geq 1$, the controller tracks the setpoint and deviates only when economically justified or unavoidable. Energy savings are therefore solely the result of the predictive control property and ahead knowledge of weather and possibly other available forecasts (e.g. occupancy or setpoint changes). Possible discrepancy between the model and the actual test-site, and its reflection on the tracking error, is handled by a disturbance estimator [25].

## III. Microgrid energy flows optimization

Microgrids or building-size smart grids are expected to become an active part of the power system that enable decentralization with increased reliability and stability [27]. Because of the economic and environmental benefits that stem from the optimal microgrid energy flow, considerable attention is directed to development of better optimization algorithms and suitable modeling frameworks [28]. Examples of MPC used in different experimentally validated microgrid environments are [29], [30], [31], [32]. Challenges and future trends for renewable energy production and storage units used in microgrids and smart grids are elaborated in [27].

In the following, we present the considered microgrid model with technical constraints on its components. We explain energy flows for a microgrid with unidirectional production and consumption units, and bidirectional storages and grid connection.

### A. Discrete-time microgrid model

When observing microgrid with a sampling time large enough to disregard the transients on its energy links, it is sufficient to observe the energy balancing condition and storages dynamics. Dynamics of a microgrid storage unit are modeled via its state-of-charge (SoC)::

$$x^\mu_{k+1} = x^\mu_k - \frac{1}{C^\mu} \left( \frac{1}{\eta^\mu_{\text{dch}}} E^\mu_{\text{dch},k} + \eta^\mu_{\text{ch}} E^\mu_{\text{ch},k} \right), \tag{6}$$

where $C$, $E$ and $\eta$ denote storage capacity, energy and efficiency, respectively. Energies and efficiencies are split to discharging and charging components ('dch' and 'ch' subscripts) such that $E^\mu_{\text{dch}} \geq 0$ and $E^\mu_{\text{ch}} \leq 0$. This is done to avoid high calculation complexity of a mixed-integer problem formulation for optimization of microgrid energy flows [9]. For MPC implementation, (6) is formulated as:

$$x^\mu_{k+1} = A^\mu x^\mu_k + B^\mu u^\mu_k, \tag{7}$$

where $x^\mu_k$ is a storages SoC vector, $u^\mu_k$ is a vector of energies exchanged between the microgrid and the storage systems between time instants $k$ and $k+1$, and $A^\mu$ and $B^\mu$ are corresponding model matrices. The model and control algorithm sampling time is selected to correspond to the sampling time of zone-level control presented in Section V.

Microgrid energy balance condition (energy conservation law on the microgrid link), satisfied at every discrete time step $k$, is:

$$E^{\text{G}}_k = E^{\text{L}}_k - \mathbf{1}_d^\top d^\mu_k - \mathbf{1}_u^\top u^\mu_k, \tag{8}$$

where $E^{\text{G}}_k$ is the energy exchanged with the utility grid, $E^{\text{L}}_k$ is the energy supplied to the load, $d^\mu_k$ is a disturbance vector of energy productions of different generation units in the microgrid and $\mathbf{1}_d$ and $\mathbf{1}_u$ are appropriately sized vectors of ones. In general, there also other non-controllable loads besides the $E^{\text{L}}$ in the building microgrid (e.g., load of electronic equipment). They can, like generation, be predicted [26] and included in the disturbance vector $d^\mu$, with negative signs.

### B. Energy flows optimization

When operating in grid-connected mode, a microgrid can import/export energy from/to the utility grid. A decision when to buy from or sell energy to the utility grid and in which amount, i.e., when to charge and discharge storages, is a complex function of the predicted microgrid load, power production (renewables), and of the current storages state-of-charge (SoC). This function is also subject to various constraints like energy storages capacity, power ratings of microgrid links to individual devices, and even to utility grid possible outage or probabilistic constraints of stochastic scenarios [9].

Storage SoC is only permitted to operate between capacity limits ($x^{\mu}_{\min}$ and $x^{\mu}_{\max}$ ), often also to avoid rapid degradation or permanent storage damage. This is put in the form of MPC state constraints:

$$x^{\mu}_{\min} \leq x^{\mu}_{k} \leq x^{\mu}_{\max}. \tag{9}$$

Power ratings of the microgrid storage links and grid connection capacity are expressed with the following constraints:

$$u^{\mu}_{\min} \leq u^{\mu}_{k} \leq u^{\mu}_{\max}, \tag{10a}$$

$$P^{\mathrm{G}}_{\min} T_s \leq E^{\mathrm{G}}_{k} \leq P^{\mathrm{G}}_{\max} T_s. \tag{10b}$$

where $T_s$ is the sampling time period.

Finally, the optimization problem for achieving the maximum economic gain of microgrid is formed as the following linear program (LP):

$$\begin{aligned} J^{\mu *} = \min_{\mathbf{u}^{\mu}} & \sum_{k=0}^{N-1} c_k E^{\mathrm{G}}_{k}, \\ \text{s.t.} \quad & (7), (8), (9), (10), \end{aligned} \tag{11}$$

where $c_k$ is the grid price for energy between the sampling instants $k$ and $k+1$. Here we assume that buying and selling prices are equal, which may not the be the case in practice. For this, the energy exchanged with the grid is separable to buying and selling amount without introducing additional integer variables [33]. Following from (11), microgrid operational conditions are imposed by the external grid through the price vector $c$ without feedback participation in the grid pricing mechanism. More elaborated version of (11) may be applied by including expected microgrid equipment wearout (mainly batteries [30]) or peak shaving ability.

## IV. Parametric hierarchical coordination

A common approach in joining the two presented MPC problems (5) and (11) is by concatenating the matrices and the cost functions of each problem into one larger control problem formulation subject to augmented model and joint constraints. However, as motivated in the Introduction, implementation with minimal on-site modifications and integration of different technologies contributes to significant cost reduction. The zone and microgrid level separation is therefore retained and the coordination is performed by exchanging information about optimized energy consumption price and consumption profiles, which are respected in both level operation. In the following, we present the proposed coordination algorithm in more details.

Parametric coordination of hierarchy levels exploits the multiparametric MPC and critical regions (CRs) with simple explicit control law. The original algorithm for multiparametric MPC was proposed in [34] and here we utilize its segments for hierarchical coordination. The distinction is that only a single CR is determined at one iteration and no additional partitioning of the parameter space is performed. For convenience, the key elements of the original work [34] used here are concisely described.

A critical region is a subset of parameters $\theta$ that yield the same set of active constraints, i.e., constraints that are satisfied with equality sign in the optimal solution. For the observed zone-level optimization (5), energy inputs per zone are control variables whereas they, summed up through all zones, act as disturbance parameters for the microgrid-level optimization (11). Zone level cumulative thermal energy demand and the corresponding microgrid electrical load are related through coefficient of performance (COP), a heating efficiency measure dependent on the outside conditions, targeted medium temperature and/or medium flow. A separate measure, energy efficiency ratio (EER), is equivalently used for the cooling process. For clarity purposes, we refer to the COP as a term for both regimes. Constant COP parameter is commonly used in MPC approaches [5], since it simplifies the problem while keeping the sufficient accuracy for the aimed purpose. Microgrid and zone levels are therefore related through thermal loads transposable to electrical load. Parameter $\theta_k$ is chosen as the sum of thermal control signals $u^{z*}$ over all zones at time $k$:

$$\theta_k = E^{\mathrm{L}}_{k} := \frac{1}{\mathrm{COP}} \sum_{j=1}^{n^{z}_{u}} u^{z*}_{j,k}. \tag{12}$$

Following from (7)–(11), the microgrid optimization problem is put in the form:

$$\begin{aligned} J^{\mu *} = \min_{\mathbf{u}^{\mu}} & \sum_{k=0}^{N-1} h^{\top}_{k} u^{\mu}_{k} + f^{\top}_{k} \theta_k, \\ \text{s.t.} \quad & \mathbf{G}\mathbf{u}^{\mu} \leq \mathbf{w} + \mathbf{L}\,\boldsymbol{\theta}, \end{aligned} \tag{13}$$

where $\boldsymbol{\theta}$ is obtained by stacking $\theta_k$ over the prediction horizon. Constraints are separated into active (A) and inactive (NA) subset for certain critical region with optimal control law $\mathbf{u}^{\mu *}$ over the prediction horizon $N$:

$$\mathbf{G}^{\mathrm{A}}\mathbf{u}^{\mu *} = \mathbf{w}^{\mathrm{A}} + \mathbf{L}^{\mathrm{A}}\boldsymbol{\theta}, \tag{14a}$$

$$\mathbf{G}^{\mathrm{NA}}\mathbf{u}^{\mu *} < \mathbf{w}^{\mathrm{NA}} + \mathbf{L}^{\mathrm{NA}}\boldsymbol{\theta}. \tag{14b}$$

From (14a) follows the linear control law with respect to $\boldsymbol{\theta}$ over the critical region $\mathrm{CR}$:

$$\mathbf{u}^{\mu *}(\boldsymbol{\theta}) = \underbrace{(\mathbf{G}^{\mathrm{A}})^{-1}\mathbf{L}^{\mathrm{A}}}_{\mathbf{D}}\boldsymbol{\theta} + \underbrace{(\mathbf{G}^{\mathrm{A}})^{-1}\mathbf{w}^{\mathrm{A}}}_{\mathbf{q}}, \quad \boldsymbol{\theta} \in \mathrm{CR}, \tag{15}$$

and corresponding linear cost function for the optimizer, called value function:

$$J^{\mu *}(\boldsymbol{\theta}) = \underbrace{\left(\mathbf{h}^{\top}\mathbf{D} + \mathbf{f}\right)}_{\mathbf{r}^{\mu}}\boldsymbol{\theta} + \mathbf{h}^{\top}\mathbf{q}. \tag{16}$$

The active critical region $\mathrm{CR}(\boldsymbol{\theta})$ is defined with:

$$\mathbf{G}_{\mathrm{CR}}\boldsymbol{\theta} \leq \mathbf{w}_{\mathrm{CR}}, \tag{17}$$

where

$$\begin{aligned} \mathbf{G}_{\mathrm{CR}} &= \mathbf{G}^{\mathrm{NA}}\mathbf{D} - \mathbf{E}^{\mathrm{NA}}, \\ \mathbf{w}_{\mathrm{CR}} &= \mathbf{w}^{\mathrm{NA}} - \mathbf{G}^{\mathrm{NA}}\mathbf{q}. \end{aligned}$$

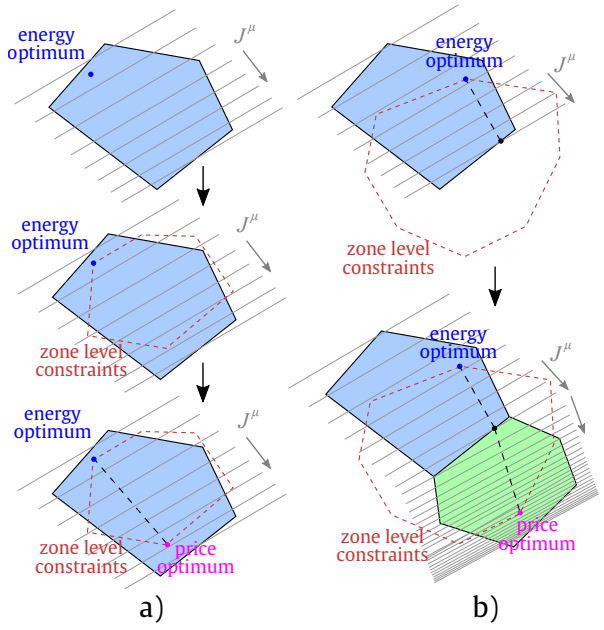


Fig. 2. Geometric representation of parametric coordination in the space of $\mathbf{u}^z$: a) solution is inside the starting CR, b) iteration to a nearby CR. Parallel lines represent the cost function with higher density reflecting a smaller value.

The zone level problem is extended to cooperate with the microgrid level by choosing:

$$\mathbf{r} = \frac{1}{\mathrm{COP}}\,\mathbf{r}^{\mu}, \tag{18}$$

and by adding (17) (combined with (12)) as additional set of constraints to modify the initial zone temperature control problem (5). Vector of parameters $\mathbf{r}$ is the $r_k$ from (5) extended over the prediction horizon. As a result, improved control signals are obtained with respect to microgrid objective, denoted with $\mathbf{u}^{z**}$. Initial solution is shifted along the decreasing value of $J^\mu$ from (16) such that all physical and comfort constraints are satisfied, which is expressed by triggering the constraints (1)–(3). Previous *energy optimal* thermal actuator inputs $\mathbf{u}^{z*}$ are now transformed to *price optimal* ones, $\mathbf{u}^{z**}$, within the critical region $\mathrm{CR}(\boldsymbol{\theta})$. Finally, the price optimal microgrid energies $\mathbf{u}^{\mu**}$ within the critical region are obtained from (15) by using (12). The method is graphically illustrated in Fig. 2.a.

This shifting of energy optimal to price optimal thermal inputs is treated as a price-sensitivity $\Delta\mathbf{u}^z$ of the building climate control:

$$\Delta\mathbf{u}^z = \mathbf{u}^{z**} - \mathbf{u}^{z*}. \tag{19}$$

The approach is based on the premises that the non-coordinated solution on the lower level is near the optimum achieved through coordination. In practice, the premise of solution proximity is also justified for the case of building connected to a variable price energy market [7]. When such assumptions are compromised, the CR boundaries are hit before the zone level constraints and the solution is to be found outside the current CR. The procedure is then iteratively executed until the solution is found in the active CR where zone level constraints are triggered (Fig. 2.b) or microgrid constraints are activated

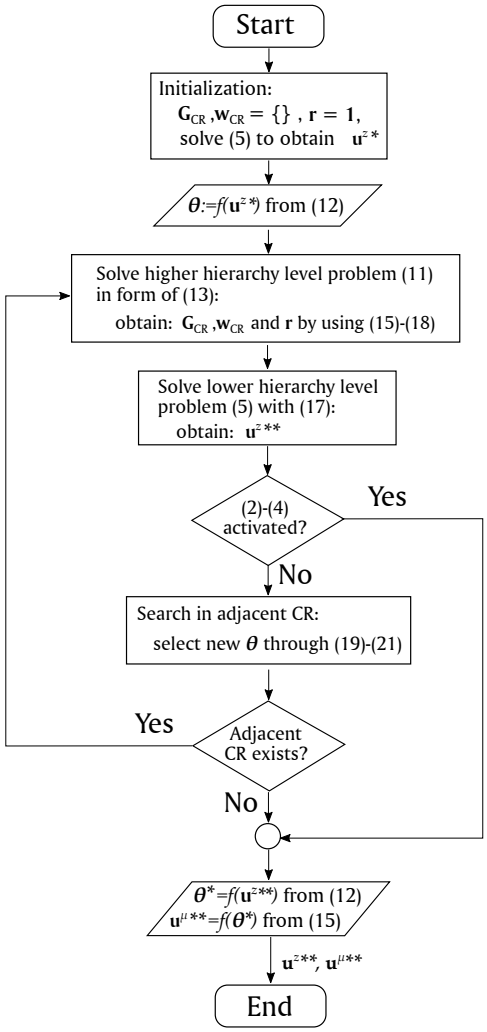


Fig. 3. Parametric hierarchical coordination flow chart.

(adjacent CR is non-existent). Mathematically, this is achieved by choosing the parameter $\boldsymbol{\theta}_{(i+1)}$ for the next iteration $(i+1)$ as:

$$\boldsymbol{\theta}_{(i+1)} = \frac{1}{\mathrm{COP}}\left(\Delta\mathbf{u}^z(\boldsymbol{\theta}^*_{(i)}) + \varepsilon\vec{u}\right), \tag{20}$$

where $\vec{u}$ is a unit vector with the direction pointed toward the price optimal solution, formulated as:

$$\vec{u} = \frac{\Delta\mathbf{u}^z}{||\Delta\mathbf{u}^z||_2}. \tag{21}$$

Parameter $\varepsilon$ is a small value (e.g. solver precision or 1% of $\Delta\mathbf{u}^z$) chosen to ensure entering into adjacent CR as a starting point for the next iteration where microgrid and zone level problems are respectively solved again. Relations (12), (17) and (18) act as an interconnection interface between hierarchy levels.

Once the solution is found in $n$ iterations, i.e., $u^{z**} \in \mathrm{CR}(\boldsymbol{\theta}_{(n)})$, microgrid price-optimal control signals $\mathbf{u}^{\mu**} = \mathbf{u}^{\mu*}(\boldsymbol{\theta}^*_{(n)})$ are calculated from (15). The overall algorithm is presented in Fig. 3 as a flow chart.

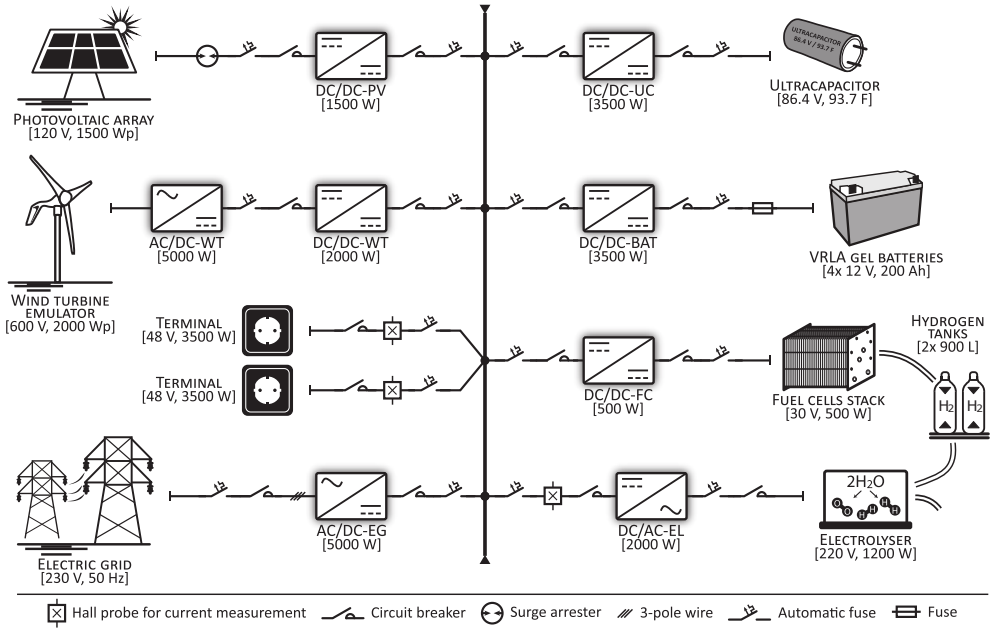


Fig. 4. Schematic topology of the considered microgrid [9].

## V. CASE STUDY

In this work, we consider a single floor of the UniZG-FEEC skyscraper building consisted of 23 controllable zones ($n_u^z = 23$), mainly offices, meeting rooms and classrooms spanning over cca. 700 m$^2$ area, equipped with two-pipe fan coils for seasonal heating or cooling. Setpoint temperatures for heating and cooling season are respectively chosen as 22°C and 24°C, according to comfort guidelines from [35]. More details about the model and used zone-level control for the considered space are given in [25].

The microgrid considered in the sequel is based on real UniZG-FEEC 48 V DC microgrid and consists of: (i) a photovoltaic array and (ii) a small-scale wind turbine emulator as power generation units, (iii) an ultracapacitor, (iv) a valve-regulated lead-acid (VRLA) batteries stack, and of (v) an electrolyzer with fuel cells stack as electricity storages, and corresponding power converters of types and powers denoted in Fig. 4. Since the ultracapacitor has a very low energy storage capacity, we neglect this component in the subsequent energy flow optimization. Regardless, it is part of the microgrid and a component that contributes to system stability for the microgrid voltage control operation. By convention, we assume that powers are positive when supplying electricity to the microgrid DC link, e.g. by discharging storages or importing (buying) energy from the utility grid. Load energy is assumed always to be unidirectional with a positive sign.

Energy productions of different sources are regarded as non-controllable disturbances $d^\mu$ with available predicted values for each time instant $k$. Weather forecast is obtained with one-hour resolution and sampling time $T_s = 1$ h is chosen for all controllers. Wind turbine and photovoltaic energy production on the prediction horizon ($E^{\mathrm{WT}}$ and $E^{\mathrm{PV}}$) are estimated from weather forecast, manufacturer data sheets and site characteristics (height and terrain roughness for wind, inclination angle for solar). For a detailed insight into the topic of system modeling and predicted energy yield, refer to [36] for wind and [37], [38] for solar energy. Vectors in (7) and (8) are therefore $x_k^\mu = [x_k^{\mathrm{BAT}},\ x_k^{\mathrm{FC}}]^\top$, $u_k^\mu = [E_{\mathrm{dch},k}^{\mathrm{BAT}},\ E_{\mathrm{dch},k}^{\mathrm{FC}},\ E_{\mathrm{ch},k}^{\mathrm{BAT}},\ E_{\mathrm{ch},k}^{\mathrm{FC}}]^\top$ and $d_k^\mu = [E_k^{\mathrm{PV}},\ E_k^{\mathrm{WT}}]^\top$. Superscript BAT denotes battery storage and FC fuel cell (hydrogen) storage related variables and parameters. Vector $d^\mu$ is also extendable to any other non-controllable load connected to the microgrid. For the current case study, we are not considering any.

Parametric hierarchical coordination applied to a particular case of zone and microgrid level control is illustrated in Fig. 5 where $\mathcal{C}^{\mathrm{CR}}$ represents critical region constraints from (17).

## VI. CLOSED-LOOP OPTIMAL CONTROL CONFIGURATIONS

To asses energy and cost saving possibilities of different controllers and configurations, mutual ground has to be established for a fair comparison. Two main identifiers are usually observed: energy spent and comfort violations, with an MPC approach compared to present baseline solutions. Since the microgrid integration and corresponding controllers are not yet adopted as a common design, we also introduce a simple baseline through a buy/sell decision-making controller suitable for future volatile pricing as well. The focus here is put on deterministic MPC with perfect knowledge of building thermal dynamics, future weather and parameters of microgrid components. All of the following zone temperature and microgrid energy flow controller outputs are energies commanded to be realized on the thermal actuators or storages up to the next sampling time instant. This approach is the key feature for ensuring a high degree of replicability by other controller types and modularity for extension to different building subsystems.

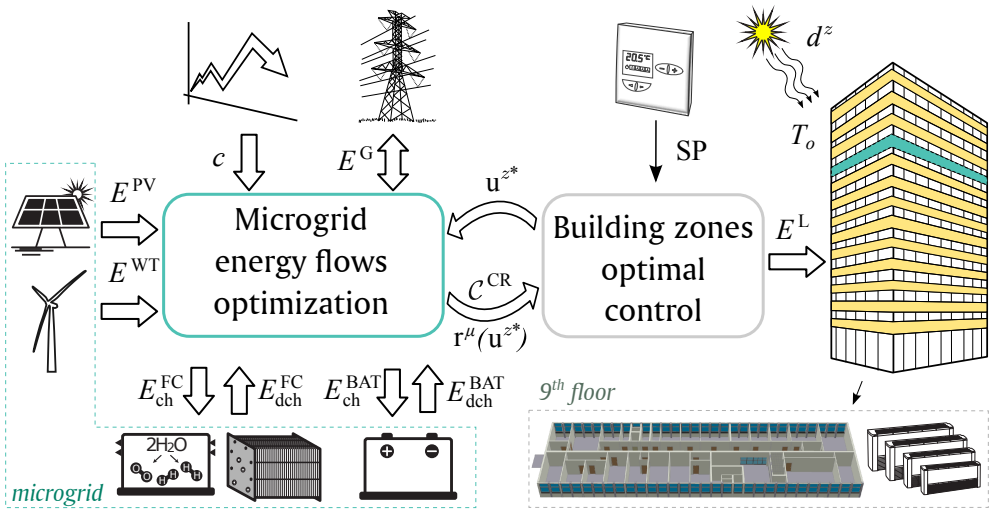


Fig. 5. Illustration of hierarchical control of the building with integrated microgrid.

The overall coordinated control and all non-coordinated MPC configurations presented in the sequel are implemented in a receding horizon fashion. At each sampling instant, the current state of the microgrid or of the zone is measured/estimated and new forecasts for any relevant data sequences are obtained. Based on the newly acquired information, the optimization is performed, control inputs $\mathbf{u}^*$ are obtained and only the first control input in the sequence ($u(t) = u^*_{k=0}$) is applied to the system.

### A. Baseline zone controller

There are several types of standard room temperature controllers such as proportional-integral (PI), rule-based or hysteresis controllers. Hysteresis controller (**HYSC**) is the most typical one and is further considered as a baseline for comparison. The considered fan coils operate at 3 different fan speeds (and switched off state) with different thermal power supply. The HYSC controller switches between available power outputs based on the difference between zone temperature and the setpoint value (set by the end-users), with allowed deviation $\Delta$ from the SP such that speed 1 is used for $\pm 0.5^\circ$C, speed 2 for $\pm[0.5, 1.5]^\circ$C and speed 3 for $\pm[1.5, 2.5]^\circ$C temperature deviations. The SP is followed only during working hours, from 7 a.m. to 6 p.m. For a fair comfort level comparison, the HYSC controller is switched on at 6 a.m. to meet the requirements of working hours in time. This configuration was in fact the one used on the considered floor of the UniZG-FEEC test site during year 2014 with the difference that the heating medium is supplied from central district heating system and COP is used for emulation of the electrical energy equivalent load during the heating season. In HYSC configuration, energy is directly taken from the grid, without microgrid level, price information or revenue possibility.

### B. Optimal zone controller

Zones MPC controller (**ZMPC**) considered here is based on the presented mathematical model and setpoint tracking problem formulation from Section II. The controller solves the problem (5) without any coordination extensions and yields the control vector sequence $\mathbf{u}^{z*}$ over the prediction horizon with $\mathbf{r} = \mathbf{1}$. Possible energy savings arise from the predictive knowledge of heat distribution throughout the building, occupancy information (working hours) and weather forecast such that unnecessary energy consumption is avoided. Typically, usual zone level controllers, such as HYSC, require the building climate system design to withstand the worst case scenario of the simultaneous peak power operation of all fan coil units. This is largely oversized in most applications and operating regimes. The constraint (4), introduced to ZMPC, highly limits the freedom of zone level operation and therefore significantly reduces possible savings when compared to HYSC. On the other hand, ZMPC allows more advanced and specific system design, which is also the case of considered microgrid operation and utility grid power converter limitations. The ZMPC configuration also takes energy directly from the grid, without microgrid level, price information or revenue possibility.

### C. Baseline microgrid controller

Based on the available building power consumption, whether from HYSC or ZMPC, a simple controller is added for microgrid energy flows balancing. A buy/sell decision-making controller is made for this purpose as a baseline for comparison with MPC methods. This so-called transactive energy controller buys the energy from the electricity grid when it is cheap and sells when it is expensive. It also utilizes the knowledge of variable pricing and exploits energy storing possibility. In hourly pricing scenario, which is available 24 hours ahead, the mean price value $\bar{c}$ is calculated as a decision-making boundary. Batteries and fuel cells are charged with the maximum possible power when electricity price is below the mean value, and discharged with the maximum possible power when above the mean electricity price value:

$$u^\mu_k = \begin{cases} (B^\mu_{\text{ch}})^{-1}(x^\mu_{\max} - A^\mu x^\mu_k), & c_k \le \bar{c} \\ (B^\mu_{\text{dch}})^{-1}(x^\mu_{\min} - A^\mu x^\mu_k), & c_k > \bar{c} \end{cases}, \qquad (22)$$

where $B^{\mu} = [B_{\text{dch}}^{\top},\ B_{\text{ch}}^{\top}]^{\top}$. The control action is then saturated at $u_k^{\mu} \in [u_{\min}^{\mu}, u_{\max}^{\mu}]$. With the mean price for decision making, controller is also valid for the case of two tariffs where storages are charged during the cheap energy and discharged during the expensive energy regime.

Whether the zone consumption follows from hysteresis or optimal controllers, the baseline microgrid controller is presented in two configurations: baseline microgrid baseline zone controller (**BMZC**) for HYSC and baseline microgrid model predictive zone controller (**BMPC**) for ZMPC.

### *D. Uncoordinated optimal zones and microgrid controller*

For the case of uncoordinated model predictive controller (**UMPC**), both zones and microgrid are controlled by model predictive controllers where optimal zone control signals are passed to the microgrid MPC as constant parameters. Electricity prices are here included in the optimization problem but are not reflected to the zone control due to the lack of coordination. The zone level consumption is therefore a non-controllable load in the microgrid.

### *E. Hierarchical optimal zones and microgrid controller*

Both zone and microgrid model predictive controllers are joined together here by the iterative parametric hierarchical coordination proposed in Section IV. Hierarchical model predictive controller (**HMPC**) exploits the knowledge of volatile pricing, yielding price optimal control signals for both microgrid converter control ($u^{\mu}(t) = u_0^{\mu **}$) and zone fan coils control ($u^{z}(t) = u_0^{z **}$), i.e., zone level consumption is a controllable load of the microgrid. When compared to UMPC, the obtained parameter vector $\theta$ is shifted from energy to cost optimum. Additional savings here arise from the predictive knowledge of electricity prices and optimal usage of energy storages. For this case, the total available building heating energy, corresponding to constraint (4), is replaced by microgrid energy balance constraint (10b). Zone level operation is tuned from energy efficient to price efficient operation. For convenience, all the considered controllers are summarized in Table I.

TABLE I
CONTROLLER CONFIGURATIONS OVERVIEW

| Controller | Zone level control | Microgrid level control |
|---|---|---|
| HYSC | Hysteresis | No microgrid |
| ZMPC | MPC | No microgrid |
| BMZC | Hysteresis | Transactive |
| BMPC | MPC | Transactive |
| UMPC | MPC | MPC |
| HMPC | MPC* | MPC |

*controllable load

## VII. SIMULATION RESULTS

Mathematical model of a UniZG-FEEC floor based on RC approach results in a total of $n_x^z = 391$ states required to model $n_y^z = 23$ zones with $n_u^z = 23$ fan coils as zone thermal actuators. Data used for external conditions are historical measurements from 2014 provided by Croatian Meteorological and Hydrological Service. States $x^z$ represent walls and zones temperatures, and disturbances $d^z$ ($n_d^z = 6$) are comprised of outdoor weather conditions (hourly radiation on exterior building walls and on north and south glazing). Physical limitations put in the form of constraints are taken from manufacturer data sheets, both for zone and microgrid level components. Photovoltaic array used in simulations is poly-Si Solvis SV60-235, wind turbine is based on Xzeres Wind Skystream 3.7 characteristics and emulated by electrical machines (turbine and generator), lead-acid batteries are First Power LFP12200G, fuel cells are polymer electrolyte membrane from the Ballard manufacturer, electrolyzer is Hogen GC 600. Central heat station is the Trane RTAC 200 HE chiller. Power converters are custom designed by research group specifications and commissioned by local manufacturer EL-UR. The data is listed in Table II, where H denotes hydrogen and all the energies (besides capacities) are related to time span between instants $k$ and $k+1$.

TABLE II
CASE STUDY PARAMETERS

| | | |
|---|---|---|
| $u_{\min}^{z}$ | -5 kWh | Max. fan coil cooling energy |
| $u_{\max}^{z}$ | 7 kWh | Max. fan coil heating energy |
| COP | 3.5 | Heating/cooling coefficient of performance |
| $u_{\min}^{z,\text{tot}}$ | -15 kWh | Max. zone level total cooling energy |
| $u_{\max}^{z,\text{tot}}$ | 15 kWh | Max. zone level total heating energy |
| $C^{\text{BAT}}$ | 10 kWh | Battery capacity |
| $C^{\text{FC}}$ | 2.5 kWh | H storage system capacity |
| $\eta_{\text{dch}}^{\text{BAT}}$ | 90% | Battery discharge efficiency |
| $\eta_{\text{ch}}^{\text{BAT}}$ | 90% | Battery charge efficiency |
| $\eta_{\text{dch}}^{\text{FC}}$ | 70% | H storage discharge efficiency |
| $\eta_{\text{ch}}^{\text{FC}}$ | 40% | H storage charge efficiency |
| $x_{\min}^{\mu}$ | $\begin{bmatrix} 10 \\ 0 \end{bmatrix}$ % | Min. battery charge state<br>Min. H storage charge state |
| $x_{\max}^{\mu}$ | $\begin{bmatrix} 100 \\ 100 \end{bmatrix}$ % | Max. battery charge state<br>Max. H storage charge state |
| $u_{\min}^{\mu}$ | $\begin{bmatrix} -3 \\ -1.2 \end{bmatrix}$ kWh | Max. battery hourly energy discharge<br>Max. H storage hourly energy discharge |
| $u_{\max}^{\mu}$ | $\begin{bmatrix} 3 \\ 0.5 \end{bmatrix}$ kWh | Max. battery hourly energy charge<br>Max. H storage hourly energy charge |
| $P_{\min}^{\text{G}}$ | -5 kW | Max. grid power when selling |
| $P_{\max}^{\text{G}}$ | 5 kW | Max. grid power when buying |
| $P_n^{\text{WT}}$ | 2 kW | Wind turbine rated power |
| $C_p$ | 0.4 | Wind turbine power coefficient [36] |
| $R$ | 1.86 m | Wind turbine blade radius |
| $P_n^{\text{PV}}$ | 1.5 kW | Photovoltaic array rated power |
| $\eta^{\text{PV}}$ | 15.9 % | Photovoltaic array power efficiency |
| $A^{\text{PV}}$ | 12.16 m$^2$ | Photovoltaic array surface |
| $\vartheta_1$ | 1.65 m$^2$ | Photovoltaic irradiance parameter [37] |
| $\vartheta_2$ | -0.23 W/K | Photovoltaic temperature parameter [37] |

Photovoltaic power profile is forecasted from available direct and diffuse solar irradiance and temperature predictions, and wind turbine power is forecasted from wind predictions. Energy market prices are obtained from publicly available European

Power Exchange company portal for 2014 [19], while the two-tariff model is the current case of building electricity provider. Simulations are performed by using MATLAB Simulink software. Model predictive control and the corresponding linear programs are solved by using the YALMIP toolbox [39] with CPLEX solver [40]. Parametric hierarchical coordination is coded within MATLAB environment based on [34] for determining CRs and handling degeneracy cases.

The cost of operation with depicted savings and revenues of each controller configuration is presented in Fig. 6 for volatile pricing case and conservative two tariffs approach in Fig. 7. The heating and cooling temperature SPs are respectively chosen as 22°C and 24°C. Bars denoted as *Total* reflect the whole year operation while *Heating* denotes only the heating period. The difference between the two are the cooling season (June 1st till September 30th) operation costs. Costs of operation are calculated from (11) as $J^{\mu} = \mathbf{c}^{\top}\mathbf{E}^{\mathrm{G}}$, i.e., the exchanged energy with the grid during each sampling time interval of 1 h is multiplied by a corresponding electricity price and accumulated for the whole year. Figures 6 and 7 also present cases of $\gamma \geq 1$ for comfort focus and $\gamma < 1$ for savings focus with given total operating costs for year 2014 with heating and cooling seasons, together with percentage savings relative to HYSC configuration. Recall that HYSC and ZMPC are not integrated to the microgrid and corresponding zone levels and therefore act as passive consumers from the grid perspective. If observing only the microgrid storages management method without zone thermal level management, UMPC and BMPC are directly comparable since both have exactly the same zone level consumption (uncontrollable load). The UMPC shows a clear contribution over BMPC and additional gains by employing predictive controller compared to a non-predictive one. The HMPC introduces additional savings with pre-heating and pre-cooling as the zone level acts as a controllable load of the microgrid. Due to renewable energy production and storages management with respect to variable prices, microgrid completely covered zone cooling/heating expenses for HMPC configuration with $\gamma < 1$ while cooling season in the most cases (BMZC, BMPC, UMPC, HMPC) resulted with revenue. This is denoted in Fig. 6 as heating expenses larger than total. The revenue is assigned to exporting of the surplus energy with same grid exchange conditions as for the energy importing case. It is also worth to note that year 2014 had a rather cold summer, which relieves zone level control and gives a large opportunity for storages management and resulting revenue. Results are given for $\gamma = 0.5$ and $\gamma = 1$, but simulations with $\gamma \in \{0, 0.75, 1.1, 1.5\}$ yielded results with less than 1% difference. Notice that HYSC and BMZC are not influenced by $\gamma$ since they are not based on the zone level MPC.

The present two-tariff pricing scenario from Fig. 7 shows similar results and contribution of each configuration. The

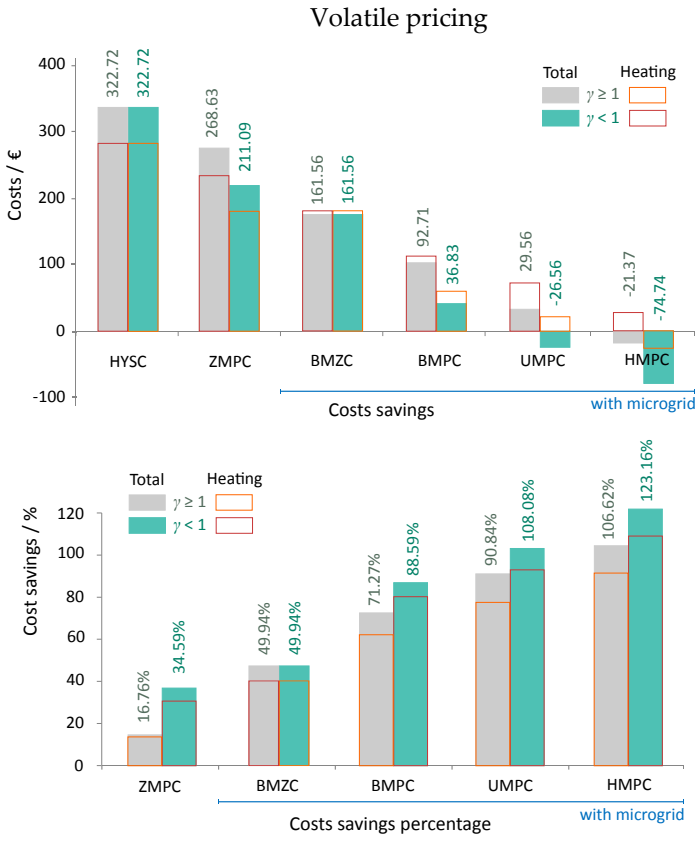


Fig. 6. Cost savings with volatile hourly prices in € and relative to currently implemented case of HYSC.

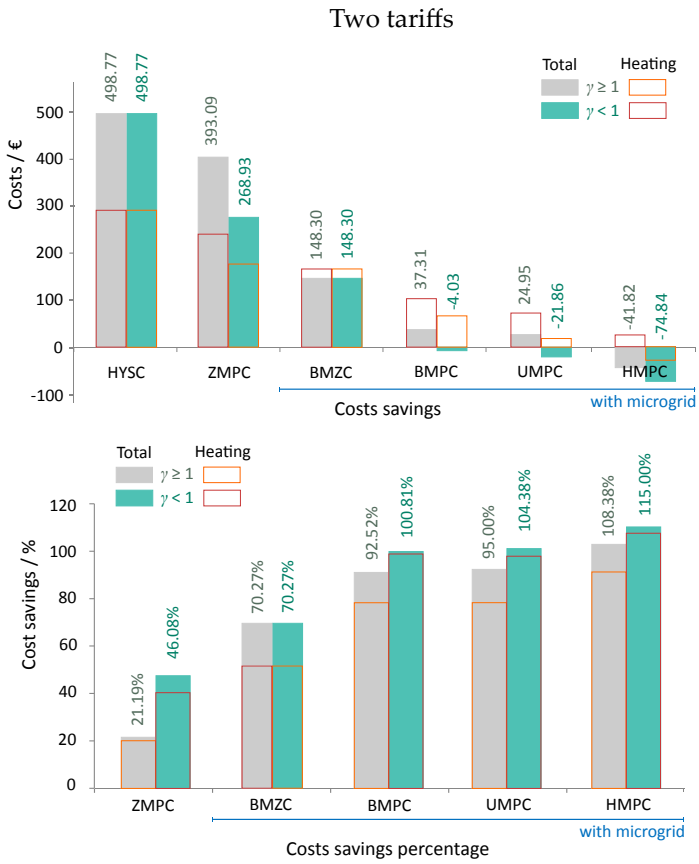


Fig. 7. Cost savings with two-tariff prices in € and relative to the present case of HYSC.

main difference is largely improved contribution of BMPC, which results in similar costs as for UMPC. Note that both are built on the same outputs of ZMPC and there is a lack of exploitation of opportunities offered by prediction due to only two possible costs of operation. Overall larger savings are due to larger difference between low and high prices, which makes the storages charge/discharge more cost-efficient. The BMPC, as a transactive energy controller, can also be extended to include more than two price levels (even up to 24), but loses its competitiveness to predictive controllers in the presence of increased market and system dynamics.

Analysis of the considered controllers performance is further presented for different weather conditions. Figure 8 presents the weather forecast for selected 6 semi-clouded days with significant temperature variation at the transition of February to March 2014 to illustrate the performance of various configurations during the heating regime. Depicted irradiances are the total incident irradiance on the south- and the north-facing building surface, where expressed peak at noon of Feb 27 is the result of a clear sunny day.

Figures 9 and 10 show the temperature response and supplied thermal energy to the exemplary considered zone for the four main controller configurations. Results are shown for volatile energy pricing scenario with selected parameter $\gamma = 1$, which imposes the equivalent weight of energy savings and reference temperature tracking. Since BMPC and UMPC are based on the same outputs of ZMPC, and BMZC on HYSC outputs, the corresponding results coincide. Intensive on/off switching of fan coil unit is clearly visible for the HYSC case with relaxation induced by sunny day external conditions. Figures also show the predictive feature of UMPC and HMPC where heating is initiated few hours in advance to satisfy comfort demands at the start of working hours. Although the behavior is similar, the cause of such ahead-schedule heating is very different. Just before the working hours start, controllers are required to simultaneously deliver peak values of thermal power to each of 23 zones while further maintaining the zones temperature during working hours requires less effort with supportive sun irradiance and higher outdoor temperature. The UMPC is largely

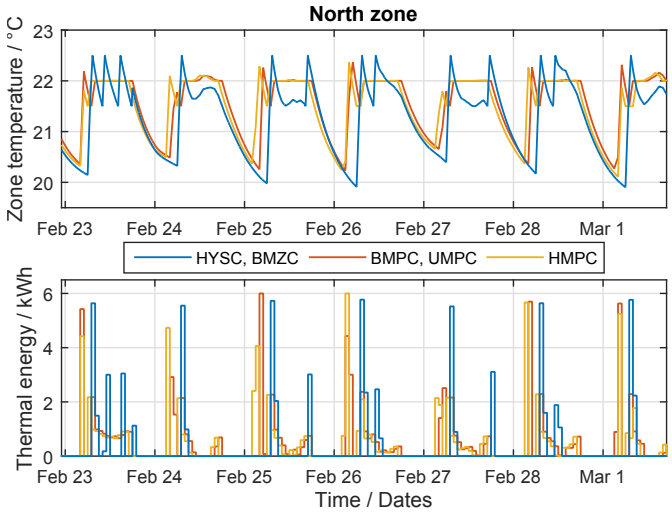


Fig. 9. North zone temperature and heating energy delivery.

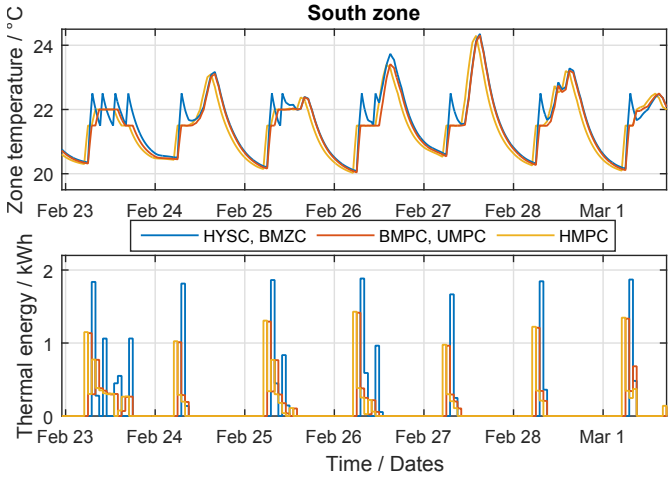


Fig. 10. South zone temperature and heating energy delivery.

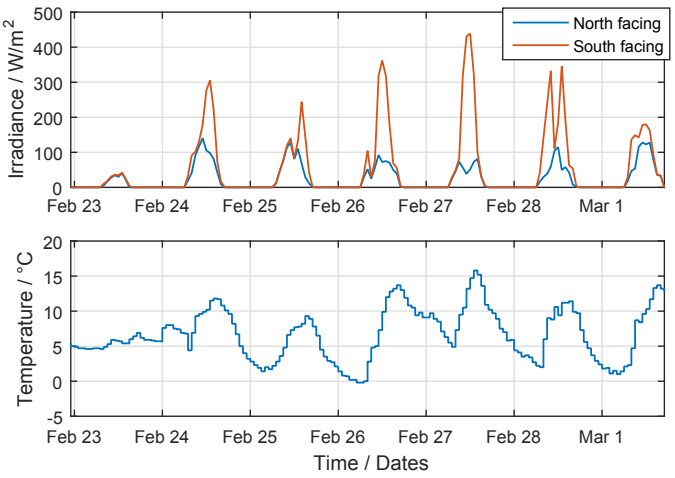


Fig. 8. Weather conditions.

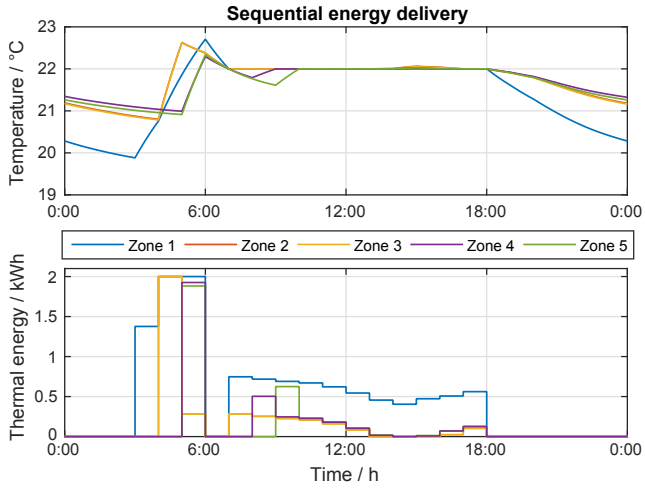


Fig. 11. Sequential energy delivery due to constraint (4) by BMPC and UMPC.

dependent on the constraint of (4) that limits the available power. The constraint is enforcing the UMPC to sequentially heat each zone and overcome the peak energy delivery demand with respect to available supply. The sequential power delivery is shown in Fig. 11 for 5 zones, where the temperature is risen up above the setpoint and then naturally cooled to match the 22°C setpoint at 7 a.m.

On the other hand, the HMPC has access to renewable production and predictive storage management that increase the available power for supporting the starting heating peak. This is expressed through the constraint (10b) with power balance condition (8). Although the requirement to cope with limited power supply is greatly eased, HMPC results in similar behavior to UMPC. This is due to significantly lower energy prices during night hours, whereas preheating is the result of cost-optimal problem formulation. It may also be observed in south zone temperature case that HMPC, compared to UMPC, imposes preheating during working hours (e.g. Feb 26, at 10 a.m.) when energy prices outmatch the setpoint tracking on the prediction horizon in the formulated optimization problem.

Figure 12 shows coinciding results of the common unified and the proposed hierarchical approach, which validates the credibility of the proposed method. Different time period is deliberately chosen to show slight deviation at hours 8-10 a.m. of Apr 9. This is the result of a so-called degeneracy case. From the cost-optimal perspective, at the given point there are more optimal solutions and both solutions from Fig. 12 are optimal and equivalent. This is verified by comparing the cost function values of the two approaches that coincide at the solver precision level ($J^{\mu**} = -0.07864$ for both approaches, at the point of largest visual difference). The difference is a result of different approaching vectors of unified and HMPC cases. For the particular case of building zone climate control, this is expected since there are many ways to equivalently preheat numerous zones while maintaining the same sum of delivered energy.

Renewable energy production, energy price profiles and resulting power exchange with the utility grid are presented in Fig. 13. The figure also presents the profile of the two-tariff scenario currently applied at the case study location. For illustrative purposes, the prices are shown with an offset of $-0.012$ € that approximately covers different taxes and duties (VAT, renewables support, grid fees etc.). The volatile prices are taken directly from the energy market and two-tariff pricing represents the final terms perceived by the consumer: $c \in \{0.0320, 0.0653\}$ €. The energy price profile is followed by all three controller types and power is exchanged with the grid by respecting the tendency of buying at low and selling at high costs, with deviations for maintaining desired comfort level.

Energy price profile and exchanged energy with the utility grid from Fig. 13 are tightly correlated with storages management as shown in Fig. 14. Because of low charging/discharging efficiency of fuel cells and the corresponding electrolyzer, the system is only used with an abundant surplus of energy (e.g. hours 2-7 p.m. of Feb 23 with significant wind turbine power production from Fig. 13), or with pronounced differences in energy prices for the case of UMPC and HMPC. Microgrid therefore mainly resides on battery storage, which is expectedly much more utilized in coordinated zone-microgrid control of HMPC. The BMPC follows only simple buy/sell decision without predictive properties and storages usage is therefore completely aligned with prices. The BMZC is omitted here for a clear illustration purpose.

Figure 15 shows the matched zone-microgrid operation on a one day scale. During the preheating period, energy drawn from the grid is mainly put to thermal demands. When zone temperature setpoint is reached and maintained, storages are charged and discharged to match the price conditions.

Results replicability is expected for different scenarios (weather conditions, case study size, reasonable microgrid components scales etc.) of a commercial building situated in

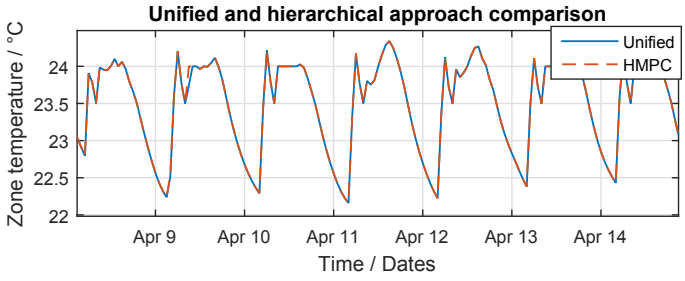


Fig. 12. Comparison of the unified and the proposed hierarchical control approach.

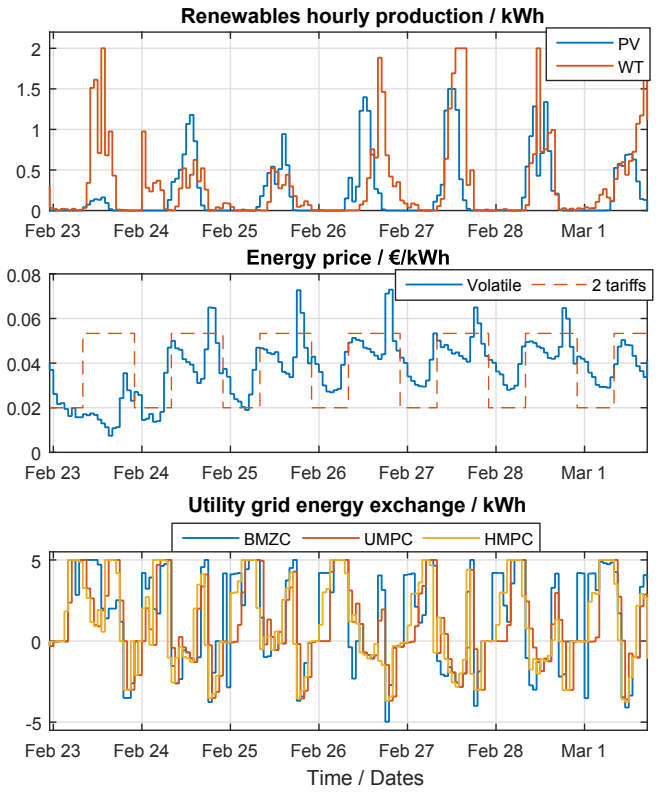


Fig. 13. Microgrid renewables production and energy exchanged with the grid.

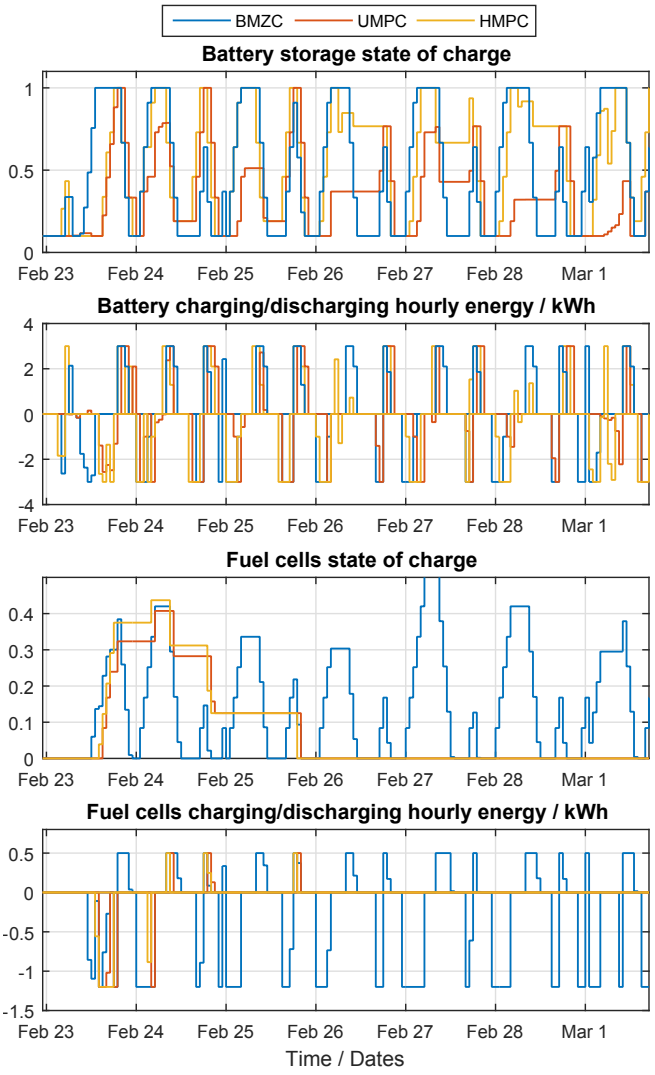


Fig. 14. Microgrid storages energy flows and state-of-charge.

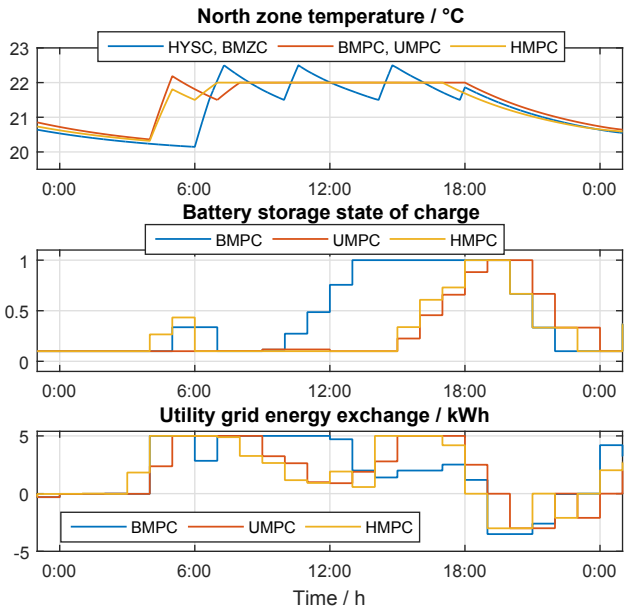


Fig. 15. Zone and microgrid operation on a one-day time scale for Feb 23.

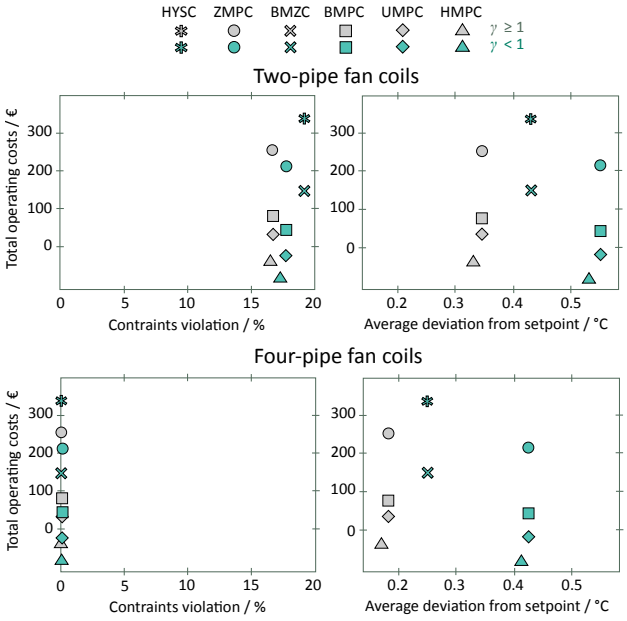


Fig. 16. Comfort level indicators for different controller configurations.

a temperate climate. The method is also suitable for other climates with common outline that predictive property of the MPC is fully exploited in highly-dynamic weather and market conditions where price profiles are received from the external grid operator without participation of the building in market pricing mechanism.

Comfort level for different controller configurations is shown in Fig. 16 and compared to the resulting cost of operation. Constraints violation, expressed in percentage, are used as a significant comfort violation indicator that is triggered in case of a deviation from SP $\pm$ $\Delta$ interval. This occurs when $\sigma_1$ or $\sigma_2$ from (2) are strictly positive, e.g. available power is insufficient for covering the peak demand or inadequate for compensating the disturbance effect. This is highly expressed for two-pipe fan coils case when outside temperature and solar irradiance are too high in the heating season or too low in the cooling season. The considered MPC approaches show better results than HYSC due to the prediction of working hours requirements and timely applied preheating/precooling. Scenario with four-pipe fan coils, typical thermal actuators in commercial buildings, is also presented in the figure for a comparison purpose. Here, there are practically no constraints violations, which is expected for the deterministic MPC approach. Deeper analysis of the ensured comfort quality level is visible as average deviation (AD) from the setpoint for different configurations. It is calculated as a ratio of the sum of all the deviation amounts during overall number of samples within working hours, for all offices in the building. The difference introduced with $\gamma$ parameter selection is evident. Here HYSC performs better from the comfort quality aspect as MPCs are saturated at $\pm\Delta$ temperature for $\gamma < 1$. The AD indicator provides information of average expected temperature in each time instant SP $\pm$ AD,

TABLE III
TWO-PIPE FC COSTS FOR SEASONAL TEMPERATURES AND $\gamma = 1$.

| 2-pipe FC | | | Operation cost / € | | | | | |
|---|---|---|---|---|---|---|---|---|
| Price | SP | Season | HYSC | ZMPC | BMZC | BMPC | UMPC | HMPC |
| Volatile | 22°C | Heating | 282.85 | 238.51 | 167.11 | 110.59 | 69.51 | 23.50 |
| | | Cooling | 59.44 | 49.65 | 14.02 | 1.37 | -20.40 | -24.71 |
| | 24°C | Heating | 357.91 | 307.65 | 241.16 | 177.33 | 142.32 | 102.22 |
| | | Cooling | 39.87 | 30.12 | -5.55 | -17.88 | -39.95 | -44.87 |
| 2-tariff | 22°C | Heating | 407.91 | 325.59 | 178.86 | 87.13 | 87.87 | 30.06 |
| | | Cooling | 132.82 | 110.25 | 11.40 | -7.08 | -20.28 | -29.61 |
| | 24°C | Heating | 518.29 | 422.63 | 289.24 | 180.05 | 187.98 | 147.23 |
| | | Cooling | 90.86 | 67.50 | -30.56 | -49.82 | -62.93 | -71.88 |

TABLE IV
FOUR-PIPE FC COSTS FOR SEASONAL TEMPERATURES AND $\gamma = 1$.

| 4-pipe FC | | | Operation cost / € | | | | | |
|---|---|---|---|---|---|---|---|---|
| Price | SP | Season | HYSC | ZMPC | BMZC | BMPC | UMPC | HMPC |
| Volatile | 22°C | Heating | 363.54 | 280.97 | 345.22 | 165.04 | 126.29 | 79.61 |
| | | Cooling | 100.48 | 60.93 | 97.82 | 13.87 | -6.76 | -8.61 |
| | 24°C | Heating | 409.81 | 333.47 | 385.61 | 217.38 | 183.63 | 131.22 |
| | | Cooling | 104.54 | 60.89 | 104.97 | 14.45 | -4.17 | -11.11 |
| 2-tariff | 22°C | Heating | 547.08 | 395.96 | 479.92 | 180.64 | 183.92 | 124.64 |
| | | Cooling | 207.42 | 124.07 | 170.55 | 9.55 | -1.53 | -12.78 |
| | 24°C | Heating | 609.55 | 466.65 | 537.15 | 252.17 | 261.02 | 196.18 |
| | | Cooling | 213.32 | 113.45 | 183.57 | -0.22 | -6.08 | -23.85 |

e.g. for HMPC with $\gamma \geq 1$, the average expected temperature during summer time is $\mathrm{SP} \pm 0.13$°C. The HMPC gives slightly better results since the applied constraint (10b) gives more flexibility than (4) as for the other cases.

A broader overview of operating costs under different configurations and user setpoints is given in tables III and IV. The simultaneous heating and cooling capability of four-pipe FCs significantly improves the temperature comfort (shown in Fig. 16) and evidently introduces additional costs.

As shown in results, comfort setpoints (i.e., the occupants behavior) significantly affects the operation costs. The potential energy savings with temperature setpoint tracking MPC reach up to 28% in different setups, as reported in [2], [3], [4]. Results here clearly show large cost-optimization opportunities of manipulations in tight comfort conditions with 34% additional savings of presented ZMPC as a similar approach.

Uncertainty handling of model variation, weather, renewable energy production or user behavior may be enhanced with robust or stochastic MPCs. More details of the building energy management system and heating/cooling medium conditioning system (central HVAC) with variable coefficient of performance or different operating regimes can be applied for more credible cost analysis.

Correlation of achieved cost-savings with expected technical equipment investments and maintenance costs including battery life expectancy can be found in [3], [27] and [41]. Additionally, negative impact of charging/discharging cycles on batteries duration can also be included in the optimization criterion [30] for more comprehensive cost-optimization.

Table V shows the proposed parametric hierarchical coordination algorithm execution speed properties for one year simulation duration. The premise of energy and price-optimal solution proximity is evident with the majority of solutions obtained within one iteration of the algorithm. Solver execution time is an averaged value for CPLEX LP solver and applied dual simplex method in majority of cases [40]. For a comparison, the equivalent unified problem required an average solver (dual simplex) time of 0.3845 s and the two approaches are comparable. The indicators are greatly dependent on problem size and character, where the proposed method is expected to provide better results with two similarly sized problems on the hierarchy levels. The largest part in the execution time is used for treating degeneracies of the CR determination, as part of the parametric algorithm from [34]. This issue is evident as the number of iterations increases. Additional improvements are possible since only a single CR is required at a time without further space partitioning. Finally, the lowest boundary for possible time expectancy is the sum of required times for solution of two problems (zone and microgrid level), which is in this case 0.2767 s in average. The proposed method is also dependent on the initialization part of the algorithm (see Fig. 3), which may for some cases result in large number of CRs for converging to the price-optimum.

TABLE V
PARAMETRIC HIERARCHICAL COORDINATION EXECUTION TIMES

| No. of iterations | No. of cases | Solver time (seconds) |
|---|---|---|
| 1 | 8054 | 0.6521 |
| 2 | 267 | 1.9563 |
| 3 | 103 | 5.7862 |
| $> 3$ | 313 | - |

## VIII. CONCLUSIONS

The paper elaborates the topic of energy management in buildings with integrated microgrids and connection to utility grid and energy market. A method for modular coordination of model predictive controllers for building zone comfort and microgrid energy flows is proposed. The modularity of the method is achieved by a simple interface between the two controllers with exchange of predicted consumption and price of operation. This enables the technology independency, cost-effective implementation and up-scaling towards the smart grid and smart city concepts where buildings play active roles.

The method is applied to a case study of 23 offices at University of Zagreb Faculty of Electrical Engineering and Computing with available integrated microgrid. Zones climate control and microgrid energy flows optimization are joined and thorough simulations are performed with weather data for 2014, real volatile market prices and current two-tariff scenarios. Several controller configurations are examined to give a realistic insight into possible cost benefits of imminent or more distant technology utilization in building energy management. Results show large cost-saving opportunities of MPCs in different configurations and highlights the proposed modular approach as a possible integration method. The achieved yearly energy costs give insight into the expected maximum gains for various commercial buildings and locations.

## ACKNOWLEDGEMENT

This work has been supported by the Croatian Science Foundation under the project No. 6731 Control-based Hierarchical Consolidation of Large Consumers for Integration in Smart Grids (3CON) and by Interreg Danube Transnational Programme through the project Smart Building – Smart Grid – Smart City (3Smart), grant DTP1-502-3.2-3Smart. The authors would also like to thank to Meteorological and Hydrological Service, Croatia, for provided historical meteorological measurements.

## REFERENCES

[1] Renewable Energy Policy Network for the 21st Century (REN21), Renewables 2016, Global Status Report, 2016.

[2] F. Oldewurtel, A. Parisio, C. N. Jones, D. Gyalistras, M. Gwerder, V. Stauch, B. Lehmann, M. Morari, "Use of Model Predictive Control and Weather Forecasts for Energy Efficient Building Climate Control", *Energy and Buildings*, vol. 45, pp. 15–27, 2012.

[3] D. Sturzenegger, D. Gyalistras, M. Morari and R. S. Smith, "Model Predictive Climate Control of a Swiss Office Building: Implementation, Results, and Cost-Benefit Analysis", *IEEE Transactions on Control Systems Technology*, vol. 24, no. 1, pp. 1–12, 2016.

[4] J. Široký, F. Oldewurtel, J. Cigler, S. Prívara, "Experimental analysis of model predictive control for an energy efficient building heating system", *Applied Energy*, vol. 88, no. 9, pp. 3079-3087, 2011.

[5] T. Žakula, P. R. Armstrong, L. Norford, "Modeling environment for model predictive control of buildings", *Energy and Buildings*, vol. 85, pp. 549–559, 2014.

[6] F. Tahersima, J. Stoustrup, H. Rasmussen and S. A. Meybodi, "Economic COP Optimization of a Heat Pump with Hierarchical Model Predictive Control", in *Proc. of the 51st Conference on Decision and Control*, Maui, HI, USA, pp. 7583–7588, 2012.

[7] F. Oldewurtel, D. Sturzenegger, G. Andersson, M. Morari and R. S. Smith, "Towards a Standardized Building Assessment for Demand Response", in *Proc. of the 52nd Conference on Decision and Control*, Florence, Italy, pp. 7083–7088, 2013.

[8] M. Brandstetter, A. Schirrer, M. Miletić, S. Henein, M. Kozek and F. Kupzog, "Hierarchical Predictive Load Control in Smart Grids", *IEEE Transactions on Smart Grid*, vol. 8, no. 1, pp. 190–199, 2017.

[9] M. Gulin, M. Vašak and M. Baotić, "Analysis of microgrid power flow optimization with consideration of residual storages state", in *Proc. of the 2015 European Control Conference*, Linz, Austria, pp. 3126–3131, 2015.

[10] D. T. Nguyen and L. B. Le, "Optimal Bidding Strategy for Microgrids Considering Renewable Energy and Building Thermal Dynamics", *IEEE Transactions on Smart Grid*, vol. 5, no. 4, pp. 1608–1620, 2014.

[11] X. Xue, S. Wang, C. Yan, B. Cui, "A fast chiller power demand response control strategy for buildings connected to smart grid", *Applied Energy*, vol. 137, pp. 77–87, 2015.

[12] C. D. Korkas, S. Baldi, I. Michailidis, E. B. Kosmatopoulos, "Occupancy-based demand response and thermal comfort optimization in microgrids with renewable energy sources and energy storage", *Applied Energy*, vol. 163, pp. 93–104, 2016.

[13] A. Roskilly, P. Taylor, J. Yan, "Energy storage systems for a low carbon future–in need of an integrated approach", *Applied Energy*, vol. 137, pp. 463–466, 2015.

[14] R. Scattolini, "Architectures for distributed and hierarchical Model Predictive Control – A review", *Journal of Process Control*, vol. 19, no. 5, pp. 723–731, 2009.

[15] E. O´Dwyer, M. Cychowski, K. Kouramas and G. Lightbody, "A Hierarchical Model-Based Predictive Control Strategy for Building Heating Systems", in *Proc. of the 25th IET Irish Signals & Systems Conference and 2014 China-Ireland International Conference on Information and Communications Technologies*, Limerick, UK, pp. 298–303, 2014.

[16] P.-D. Morosan, R. Bourdais, D. Dumur, J. Buisson, "Building temperature regulation using a distributed model predictive control", *Energy and Buildings*, vol. 42, no. 9., pp. 1445-1452, 2010.

[17] S. Koehler, C. Danielson and F. Borrelli, "A Primal-Dual Active-Set Method for Distributed Model Predictive Control", in *Proc. of the American Control Conference*, Chicago, IL, USA, pp. 4759–4764, 2015.

[18] N. Parikh and S. Boyd, "Block splitting for distributed optimization", *Mathematical Programming Computation*, vol. 6, no. 1, pp. 77–102, 2014.

[19] European Power Exchange. [Online]. Available: www.epexspot.com

[20] Y. Ma, A. Kelman, A. Daly and F. Borelli, "Predictive Control for Energy Efficient Buildings with Thermal Storage: Modeling, Stimulation, and Experiments", *IEEE Control Systems Magazine*, vol. 32, no. 1, pp. 44–64, 2012.

[21] Y. Ma, J. Matuško, F. Borrelli: Stochastic Model Predictive Control for Building HVAC Systems: Complexity and Conservatism, *IEEE Transactions on Control Systems Technology*, vol. 23, no. 1, pp. 101–116, 2015.

[22] P. O. Fanger, "Thermal Comfort", Danish Technical Press (republished by McGraw-Hill, New York, 1973), 1970.

[23] American Society of Heating Refrigerating and Air-Conditioning Engineers, "2009 ASHRAE Handbook, Fundamentals", 2009.

[24] A. S. O. Ogunjuyigbe, T. R. Ayodele, O. A. Akinola, "User satisfaction-induced demand side load management in residential buildings with user budget constraint", *Applied Energy*, vol. 187, pp. 352-366, 2017.

[25] A. Martinčević, M. Vašak and V. Lešić, "Model Predictive Control for Energy-saving and Comfortable Temperature Control in Buildings", *Proc. of the 24th Mediterranean Conference on Control and Automation*, pp. 298–303, 2016.

[26] M. Gulin, M. Vašak, G. Banjac, T. Tomiša, "Load Forecast of a University Building for Application in Microgrid Power Flow Optimization", *Proc. of the IEEE International Energy Conference, EnergyCon*, pp. 1284–1288, 2014.

[27] F. Blaabjerg, D. M. Ionel, "Renewable Energy Devices and Systems State-of-the-Art Technology, Research and Development, Challenges and Future Trends", *Electric Power Components and Systems*, vol. 43, no. 12, pp. 1319–1328, 2015.

[28] A. Parisio, E. Rikos, L. Glielmo, "A Model Predictive Control Approach to Microgrid Operation Optimization", *IEEE Transactions on Control Systems Technology*, vol. 22, no. 5, pp. 1813-1827, 2014.

[29] P. O. Kriett, M. Salani, "Optimal control of a residential microgrid", *Energy*, vol. 42, no. 1, pp. 321–330, 2012.

[30] A. Parisio, E. Rikos, G. Tzamalis, L. Glielmo, "Use of model predictive control for experimental microgrid optimization", *Applied Energy*, vol. 115, pp. 37–46, 2014.

[31] G. Comodi, A. Giantomassi, M. Severini, S. Squartini, F. Ferracuti, A. Fonti, D. Nardi Cesarini, M. Morodo, F. Polonara: "Multi-apartment Residential Microgrid with Electrical and Thermal Storage Devices: Experimental Analysis and Simulation of Energy Management Strategies", *Applied Energy*, vol. 137, pp. 854–866, 2015.

[32] M. Fiorentini, J. Wall, Z. Ma, J. H. Braslavsky, P. Cooper, "Hybrid model predictive control of a residential HVAC system with on-site thermal energy generation and storage", *Applied Energy*, vol. 187, pp. 465-479, 2017.

[33] M. Gulin, A. Martinčević, M. Vašak, V. Lešić, "Multi-level Optimal Control of a Microgrid-supplied Cooling System in a Building", *Proceedings of the IEEE PES Innovative Smart Grid Technologies Conference Europe*, pp. 6, 2016.

[34] F. Borrelli, A. Bemporad, and M. Morari, "Geometric Algorithm for Multiparametric Linear Programming", *Journal of Optimization Theory and Applications*, vol. 118, no. 3, pp. 515–540, 2003.

[35] EN 15251:2007, "Indoor environmental input parameters for design and assessment of energy performance of buildings addressing indoor air quality, thermal environment, lighting and acoustics", 2007.

[36] L. Y. Pao, K. E. Johnson, "Control of Wind Turbines: Approaches, Challenges, and Recent Developments", *IEEE Control Systems Magazine*, vol. 31, no. 2, pp. 44–62, 2011.

[37] M. Gulin, T. Pavlović, M. Vašak, "Photovoltaic panel and array static models for power production prediction: Integration of manufacturers and on-line data", *Renewable Energy*, vol. 96, pp. 399–413, 2016.

[38] M. Gulin, T. Pavlović, M. Vašak, "A one-day-ahead photovoltaic array power production prediction with combined static and dynamic on-line correction", *Solar Energy*, vol. 142, pp. 49–60, 2017.

[39] J. Löfberg, "YALMIP: A Toolbox for Modeling and Optimization in MATLAB" in *Proc. of the 2004 IEEE International Symposium on Computer Aided Control Systems Design*, Taipei, Taiwan, pp. 284–289, 2004.

[40] IBM Corp., "IBM ILOG CPLEX Optimization Studio: CPLEX Users Manual", ver. 12.6., 2015.

[41] R. Dufo-López, J. M. Lujano-Rojas, J. L. Bernal-Agustín, "Comparison of dfferent lead-acid battery lifetime prediction models for use in simulation of stand-alone photovoltaic systems", *Applied Energy*, vol. 115, pp. 242–253, 2014.